ELSEVIER

Journal of Chromatography A, 707 (1995) 35–43

JOURNAL OF CHROMATOGRAPHY A

Numerical simulation of hydrodynamic dispersion in random porous media

Nicos S. Martys

National Institute of Standards and Technology, Building Materials Division, Gaithersburg, MD 20899, USA

Abstract

In this paper we present results demonstrating the utility of computational methods to numerically simulate and visualize hydrodynamic dispersion in random porous media. The role of Peclet number in the spread of a dye through porous media is illustrated. From examination of concentration profiles, effective diffusion coefficients were numerically determined for different Peclet numbers. In contrast to the case of fluid-driven dispersion, we discuss the spread of a dilute concentration of ions driven by an electric field. We also consider a simple model of size exclusion chromatography where materials that advect and diffuse through pore space also diffuse through the solid matrix.

1. Introduction

The flow and spread of fluids through random porous media such as soils, bead packings, ceramics and concrete plays an important role in a wide variety of environmental and technological processes [1,2,4]. Examples include: the spreading and clean up of underground hazardous wastes, oil recovery, separation processes such as chromatography and catalysis, and the degradation of building materials. While the study of miscible flow in porous media has been the subject of considerable research, it is difficult to obtain exact solutions of the Navier–Stokes and hydrodynamic dispersion equations for the case of flow in random porous media. However, recent advances in computers have made it possible to numerically simulate fluid flow in complex geometries. Many factors which control the invasion of fluids such as viscosity, surface tension forces, the structure of the porous medium, and the external driving force which displaces the fluids can be directly incorporated into computations of fluid dynamics [1–13].

Suppose a porous medium is saturated with a Newtonian fluid. A pressure gradient is applied across the medium maintaining steady flow. The fluid flow is assumed to be in the limit of low Reynolds number. If we now introduce a miscible dye at the side from which the fluid is entering, the dispersion or spread of the dye is locally described by the advection–diffusion equation [3–4]

$$\frac{\partial c}{\partial t} + v \cdot \nabla c = D_m \nabla^2 c \tag{1}$$

Here c is the concentration of the dye, v is the local fluid velocity, and D_m is the molecular diffusion constant. A dimensionless number which is useful to characterize the competition between diffusion and advection in the spread of a dye is the Peclet number [3] $Pe = \langle v \rangle l / D_m$ where $\langle v \rangle$ is the average fluid velocity and l is a length scale which depends on the pore geome-

SSDI 0021-9673(95)00204-9

try. When Pe is small, the diffusion process dominates the spread of the dye; at large Pe, advection dominates.

At length scales much larger than the typical pore size, hydrodynamic dispersion is generally described by the macroscopic advection–diffusion equation (2D) [3]

$$\frac{\partial C}{\partial t} + V \cdot \nabla C = D_L \frac{\partial C}{\partial x^2} + D_T \frac{\partial C}{\partial y^2} \tag{2}$$

where C is the macroscopic mean concentration, D_L and D_T are the longitudinal and transverse dispersion coefficients respectively, V is the macroscopic mean velocity, and x is in the direction of the mean flow. The macroscopic advection–diffusion equation is valid when the squared width of the dispersion front scales linearly with time. When the squared width scales nonlinearly, dispersion is called anomalous [16–18].

Previous theoretical work [14,16–18] concerning scaling in hydrodynamic dispersion through a disordered porous medium has largely focused on the understanding of anomalous dispersion and the prediction of D_L and D_T as a function of Pe and pore geometry. Here, considerable progress [14] has been made by applying: percolation concepts [14] to dispersion in random network models of porous media, mutliple scale expansions [17] (or homogenization) or by simulation of dispersion [17], at the pore scale via the convected Brownian motion of particles.

In this paper we present results demonstrating the utility of computational methods to numerically simulate and visualize hydrodynamic dispersion in random porous media. The role of Peclet number in the spread of a dye through porous media is illustrated. From examination of concentration profiles, effective diffusion coefficients were numerically determined for different Peclet number. We also consider a simple simulation model of size exclusion chromatography where an advecting dye is allowed to diffuse through the solid matrix as well as through the pore space. In this model, it is assumed that there are two dispersing materials made of, for instance, two different sized polymers. By not allowing one material (composed of the larger of the two polymers) to diffuse in the solid region in one simulation and allowing the other material (composed of the smaller of the two polymers) to diffuse in the solid region in a second simulation it is possible to compare how these different materials are transported in the same porous medium.

Finally, since it is quite common to draw an analogy between fluid flow [19,20] and flow of electrical current, results from dispersion due to an electrically driven dilute concentration of ions are given for comparison to hydrodynamic dispersion. We show that there is a dramatic difference between equal concentration contours of ions driven by an electric field and those driven hydrodynamically.

Section 2 summarizes the numerical techniques and describes the modeled porous media studied. Section 3 presents results of simulations. Finally, Section 4 further discusses the results and presents conclusions.

2. Numerical calculations

2.1. Models of porous media

This paper will mostly focus on dispersion through two-dimensional porous media constructed by randomly placing digitized discs on a lattice such that they do not overlap. The discs have diameter 13, in units of lattice spacing, and the number of packed discs is such that the porosity, $\phi = 0.8$. Typical system size was 300×300 lattice spacings. For a qualitative comparison of hydrodynamic dispersion in different porous media, cases where the porosity is very high (dilute concentration of discs) and where the porosity is near a percolation threshold are also considered. In the former case the porous medium is constructed with nonoverlapping discs having diameter 13 but with $\phi = 0.95$ and in the latter, the porous medium is constructed by randomly overlapping discs of diameter 23 such that $\phi = 0.4$.

2.2. Summary of numerical methods

Fluid flow

In the limit of slow incompressible flow, steady-state fluid flow is described by the linear Stokes [3] equations

$$\eta\nabla^2 v(r) = \nabla p(r) \tag{3a}$$

$$\nabla \cdot v(r) = 0\,, \tag{3b}$$

where v and p are, respectively, the local velocity and pressure fields, η is the fluid viscosity and r is the location. The fluid velocity must vanish at pore–solid interfaces and a pressure difference is applied at the inlet and outlet faces. To numerically solve the Stokes equations, we use a finite-difference scheme in conjunction with the artificial compressibility relaxation algorithm [19,21]. The pore space is discretized into a marker-and-cell (MAC) mesh [21], where pressures are defined at the nodes and fluid velocity components are defined along the center of bonds connecting nodes. Each pixel, a unit square representing either pore or solid, is centered on a node. Near the pore–solid interface, non-centered difference equations are used to improve the accuracy of the solution and to force the fluid velocities to zero at the true pore–solid interface, which is half way in between the nodes. As a result, velocity profiles across pixels are accurate to at least second order[a].

2.3. Advection–diffusion

For finite Pe, the advection–diffusion equation was solved numerically using finite difference methods [21,22]. The local concentration was specified on the nodes of the same MAC mesh used in the fluid flow simulation. An advantage of using the MAC mesh is that it naturally forces conservation of matter throughout the porous medium. To improve numerical accuracy and prevent oscillations in concentration which may appear due to steep gradients in concentration, we adopted the Barton [23–25] scheme in solving the advection–diffusion equation. Periodic boundary conditions were imposed along the sides parallel to the main flow direction. At the outlet the boundary condition $\partial c/\partial x = 0$ was maintained. Initially, the dye concentration is zero throughout the porous medium. A fixed dye concentration is introduced at the inlet and spreads according to Eq. 1 until the pore space is nearly saturated with dye.

In the case where we allow dispersion through the solid matrix as well as through the pore space we simply required that the mass current be continuous at the pore–solid interface. This was guaranteed by imposing the following boundary condition:

$$D_p\, \partial C/\partial x\big|_p = D_s\, \partial C/\partial x\big|_s \tag{4}$$

where D_p and D_s are the microscopic diffusion coefficients in the pore and solid space respectively, and the derivatives are evaluated in the respective pore and solid regions near the pore–solid interface [15].

3. Results

3.1. Pattern formation as a function of Peclet number

Fig. 1 shows dispersion patterns formed by an invading dye for the case where $\phi = 0.8$ and $Pe \approx 0$, 1, and 80 (Fig. 1a,b,c, respectively). Here the length scale in Pe is the disc radius. Clearly, at the lowest Pe, diffusion dominates pattern formation. Contours of equal concentration generally form a single-valued function with respect to a line drawn along the inlet. The small local variation in concentration profiles is due to the presence of impenetrable discs and relatively small fluctuations in the velocity fields. As Pe increases, advection begins to dominate and fingers form (or channeling develops) as the dye advances through channels where the fluid

[a] Suppose that, within a given pixel, we were to expand the exact solutions of the Stokes equations $v(r) \equiv v(x,y,z)$ as a Taylor series in x,y. The use of non-centered difference equations guarantees that our solutions properly represent the first three terms of this expansion (i.e., that the errors are of order x^3 or x^2y etc.).

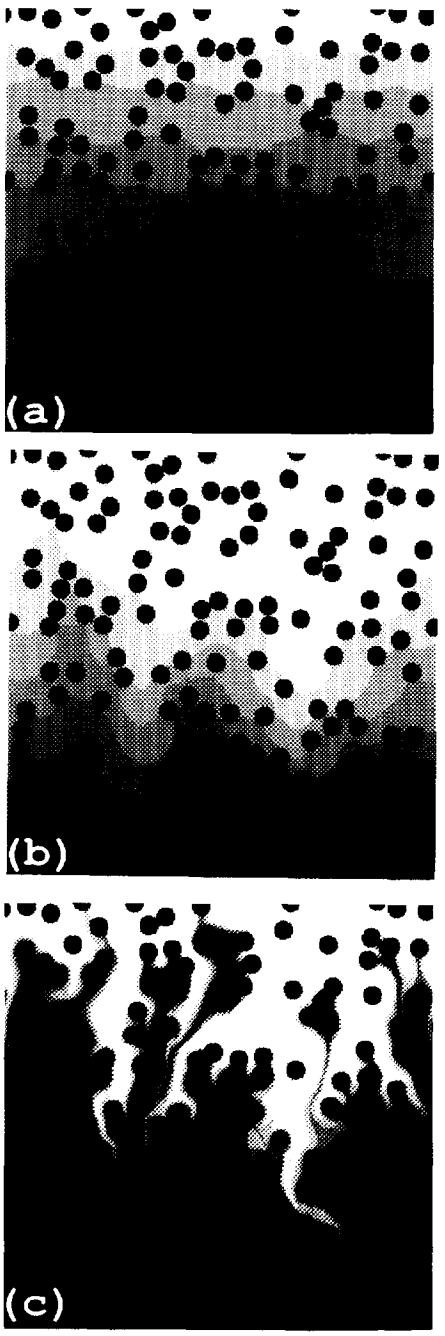

Fig. 1. Panels a–c show snapshots of pattern formation in hydrodynamic dispersion for $Pe \approx 0$, 1, and 80, respectively. Dye concentration scales such that white corresponds to $c = 1$ and black to $c = 0$. The porous medium was initially saturated with a black fluid. A white diffusing dye then enters from the top. While our simulations treat the concentration as a continuum, it is depicted here at threshold steps to reveal contours of equal concentration.

velocity is greatest. Slow flow velocity regions take much longer to invade because the dye enters primarily by diffusion. At the highest Pe, well defined fingers form as the dye follows the winding tortuous path of the fluid. Experimental studies [29] of hydrodynamic dispersion in etched networks are in qualitative agreement with our simulations.

In Fig. 2 we show different time–concentration profiles for the $Pe = 0$ case. Here the concentration is averaged over strips in the direction transverse to the ingress. The concentration is normalized by the porosity in each strip so that $C(x) = 1$ when the pore space is completely saturated. Note that when $Pe = 0$, the macroscopic diffusion coefficient D_b may be obtained from the Nernst–Einstein relation:

$$\frac{D_b}{D_m} = \frac{\sigma_b}{\phi\sigma_f} \tag{5}$$

where given a porous medium that is saturated with a conducting fluid, σ_f is the conductivity of the fluid, σ_b is the bulk conductivity of the entire medium and we assume the solid region has zero conductance. In Fig. 2 we also show the solution

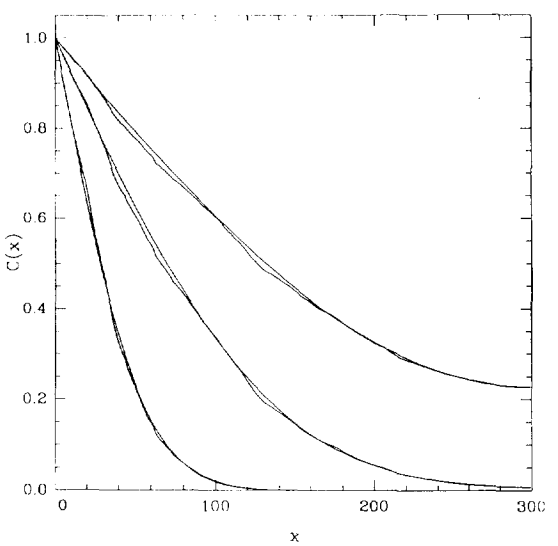

Fig. 2. Concentration profiles at different times for $Pe = 0$. The dashed line is from the solution of Eq. 2 using the macroscopic diffusion coefficient predicted by the Nernst–Einstein relation and the independently computed conductivity.

of Eq. 2 in one dimension where the longitudinal diffusion coefficient is set equal to D_b. Here D_b was obtained from the Nernst–Einstein relation after the conductivity of the system was independently determined (for more details concerning the determination of conductivity in random porous media see Ref. [19]). For the porous medium studied we found $D_b/D_m \approx 0.75$. Clearly our simulations are consistent with the prediction of the Nernst–Einstein relation.

Fig. 3 shows concentration profiles from the case where $Pe \approx 1$. Also included are solutions of Eq. 2 where the velocity $V = \langle V \rangle_p$ is only averaged over the pore space in order to correctly account for the motion of the dye which is limited to the pore space. To fit data to solutions of Eq. 2 we used the value $D_b/D_m = 2$.

At $Pe = 80$, the concentration profiles were much more difficult to fit to solutions of Eq. 2. This is a result of the sensitivity of the invasion pattern to the arrangement of the discs, long range correlations in the velocity fields as well as the existence of relatively large regions where the velocity fields are small compared to the faster moving channels. While averaging over enough samples (or a larger system size) would reduce this effect, it is necessary that the dispersion take place over a long enough time for the dye to properly sample the pore space in order to accurately determine D_b. From long time limits of the concentration profile and also from the examination of larger system sizes (300×900 and 1024×1024) we found that $D_b/D_m \approx 200$. Further studies are needed to more accurately determine D_b/D_m for this class of porous medium at high Pe. Other methods, where the convection of Brownian particles is simulated to study dispersion, may be more appropriate for the high Pe regime [4].

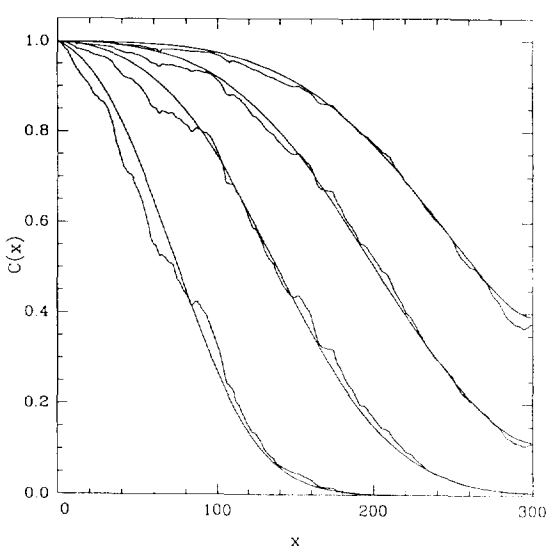

Fig. 3. Concentration profiles for $Pe \approx 1$. Also shown are fits from the solution of Eq. 2.

3.2. Dispersion in other model porous media

As a qualitative illustration of the important role pore structure plays in dispersion, two examples of dispersion are shown, to contrast with the previous simulations. Fig. 4a shows dispersion in the overlapping disc model where $\phi = 0.4$. For this model, we are near the percolation threshold for the discs, i.e. the overlapping discs form a connected cluster that spans across the system. In this regime the size of the clusters establishes the length scale (as opposed to the radius of the discs) which would appropriately define Pe. Also note, near the percolation threshold, the fewer pathways that span the system make a significant contribution to flow. Large pockets or regions where there is negligible fluid flow take very long times to saturate. The dye mainly enters these pockets by diffusing through a tortuous path. In this regime, anomalous dispersion [30] is expected to take place.

Results from the opposite extreme, of dispersion in highly porous media, are given for the case of $\phi = 0.95$ and $Pe = 25$ in Fig. 4b. Clearly the flow fields are correlated over very large distances compared to the size of the disc. This leads to the formation of very long and broad fingers. It is surprising, even in this very dilute case, how nonuniform the dispersion front is. Again, simple use of disc size is not sufficient to define Peclet number. Instead, the spacing between discs or the distance the velocity field is correlated, obtained from two-point fluid velocity correlations [19], may be more suitable.

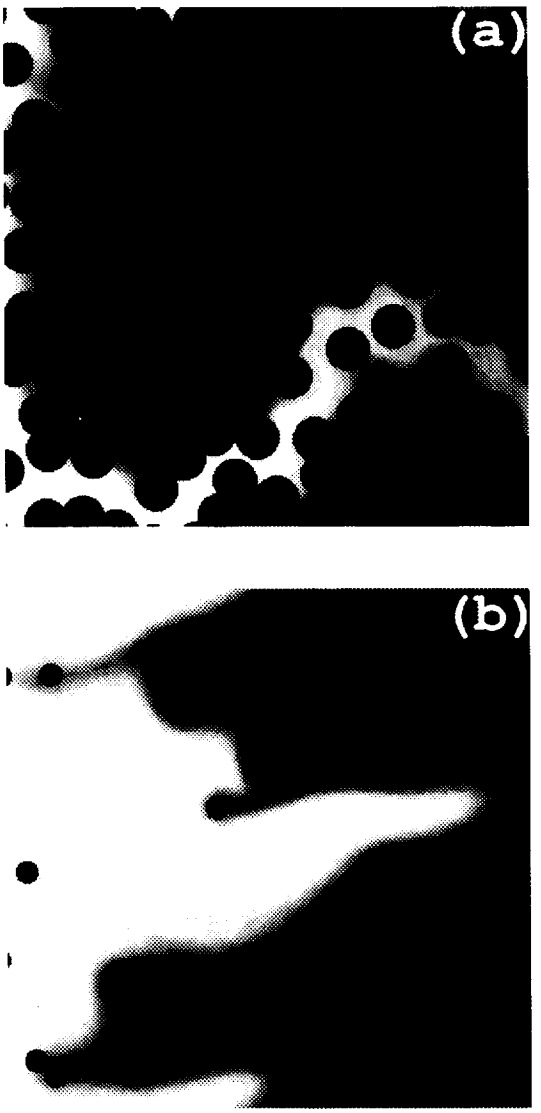

Fig. 4. Examples of dispersion through porous media in the limit where the pore space is near its percolation threshold (panel a) and in the opposite limit where the solid fraction is only 5 percent (panel b).

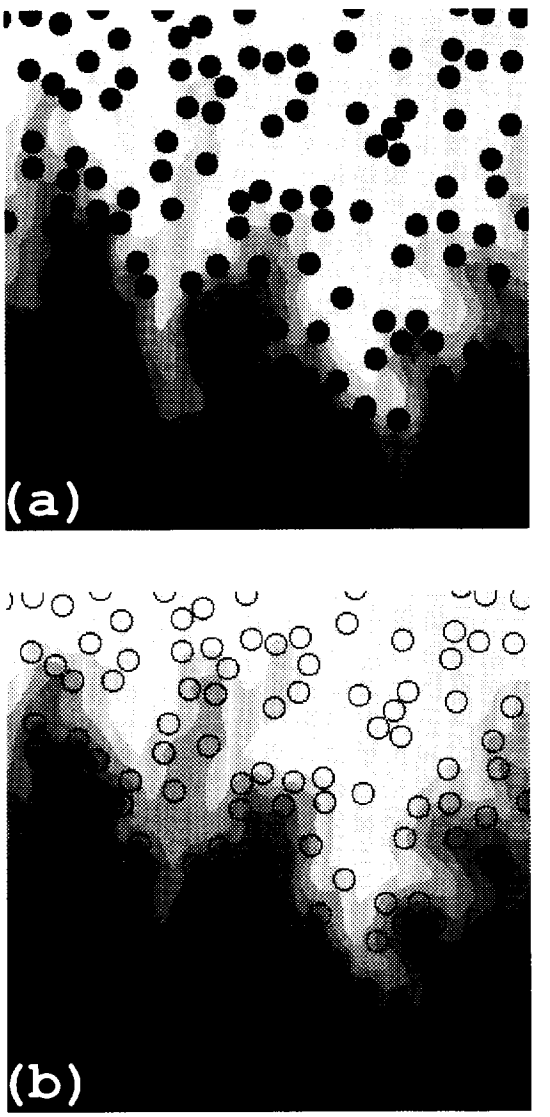

Fig. 5. Comparison of dispersion in the case where the dye is excluded from entering the solid matrix (a) and where diffusion also takes place in the solid (b). In (a), $Pe \approx 20$.

3.3. Dispersion in both pore and solid regions

Fig. 5 compares pattern formation resulting from hydrodynamic dispersion in pore space only (a) and where diffusion is included in the solid regions (b). The fluid velocity is the same in both cases and the images represent a snapshot of the dye pattern after identical time periods. The Peclet number is approximately 20 and the microscopic diffusion coefficient of the ingressing material is a factor of two higher in the pore space than that in the solid region. Clearly, when diffusion is permitted in the solid region the dye does not advance as quickly as when it is excluded from the solid region. In this case, the dye is temporarily diverted from the faster flow

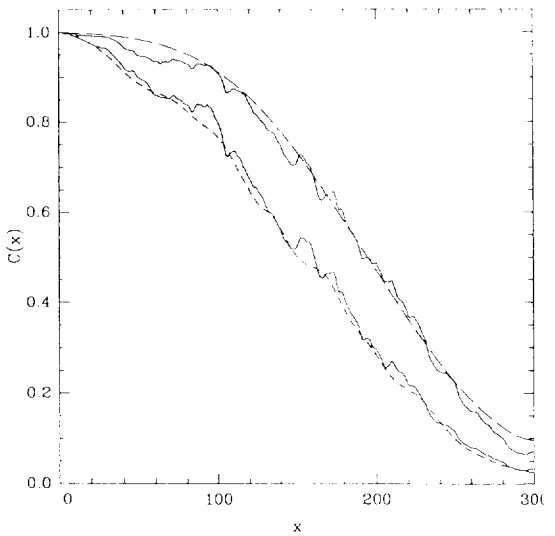

Fig. 6. Concentration profiles of the invasion patterns shown in Fig. 5. The upper solid line is the concentration profile for Fig. 5a and the long dashed line is a fit to that concentration profile using Eq. 2. The lower solid line is the concentration profile associated with Fig. 5b where only the pore space is considered. The short dashed line is the concentration profile for the entire system (pore and solid) in Fig. 5b.

regions of the fluid-saturated pore space and subsequently falls behind the dye that is excluded from the solid. Such a process is similar to that found in size exclusion chromatography.

Fig. 6 compares the concentration profiles for the previous Fig. 5. Again it is clear that the solid exclusion case permits a greater flux of material. In the case where diffusion is allowed in the solid regions there is little difference in the concentration profiles when averaging the concentration over the pore space only, or whether averaging over the entire sample, including solid regions. This is largely due to the concentration being continuous throughout the entire medium and to there not being a great difference in the diffusion coefficients associated with the solid and pore regions.

3.4. *Electrically driven concentration*

Finally, a comparison is made between the previous dispersion pattern due to fluid flow (Fig. 5a) and the dispersion of a dilute ion concentration driven by an applied electric field

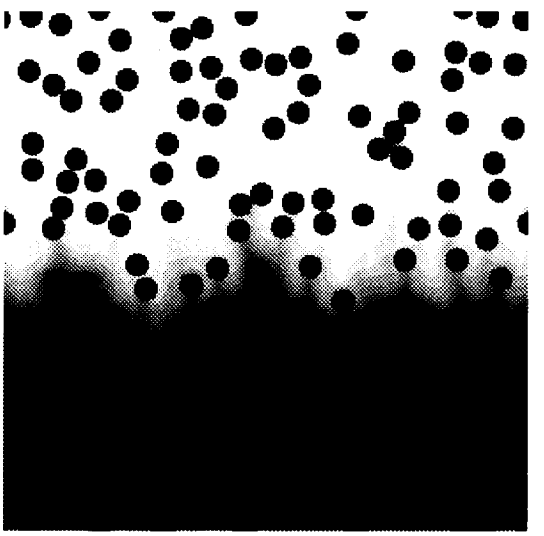

Fig. 7. Dispersion of a dilute concentration of ions where $Pe = 25$. Note the dramatic difference in the invasion pattern as compared to Fig. 5a.

(Fig. 7). Here, the same pore space used in Fig. 5a is filled with a conducting fluid. The discs are assumed to be insulating and uncharged [27]. A potential gradient is applied across the system and the Laplace equation is numerically solved to determine the electric potential everywhere. The local electric fields E are obtained from the negative gradient of the potential. Next, a dilute concentration of ions is introduced at the inlet. The ion velocity is given by $v_i = \nu zFE$ where ν is the ion mobility, z is the ion charge number, and F is Faraday's constant [28]. The dispersion of the ions is then described by Eq. 1 where c represents the ion concentration and v_i is the ion velocity as given above. We define an effective Pe for the electrically driven case by using the ion velocity in the usual definition of Peclet number.

Clearly, the patterns formed by the two driving forces, for similar Pe, are quite different. It is not unusual to find textbooks [26] that explain fluid flow in terms of electric current and vice versa and that explain Darcy's law as a type of Ohm's law for fluid flow. However, there are several important differences, at the microscopic scale, between the electric fields and flow fields in these simulations.

Consider first the fluid case. Note that the fluid velocity is zero along the pore–solid boundary. In addition, the solution of Stoke's equation will typically produce a velocity profile, between neighboring discs, that is roughly parabolic. Therefore, there is very little flow in regions only accessible to pores with narrow necks and most of the fluid flow is through the set of largest pores that form a connected path across the porous medium [19]. As a result, a dispersing dye in this porous medium may form long fingers as it moves through the faster channels, while only slowly entering regions accessible through narrow necks.

In contrast to fluid flow, the calculated electric fields need be zero only normal to the solid surface. Also, the solution of Laplace's equation results in an approximately constant electric field between discs. Thus, in the electrically driven case, there is significant movement of ions through both the narrow and wide pores such that no portion of the front greatly advances relative to another. As a result there is a more uniform displacement of ions then in the equivalent fluid case.

4. Summary

In summary, we have demonstrated the utility of real-space numerical simulation of hydrodynamic dispersion in random porous media. The study of pore scale process can lead to a clearer understanding of a variety of larger scale phenomena including the determination of macroscopic diffusion coefficients, channeling and the separation of materials as a function of pore structure and Peclet number. Although the results presented in this paper concern hydrodynamic dispersion in model porous media, the methods used here are easily extendable to more realistic pore structures and many other complex processes including surface reactions. Furthermore, we have carried out similar studies in three dimensions, results of which will be presented in a future publication.

Acknowledgements

The author would like to thank Donald Koch, Joel Koplik, Roland Lenormand, Howard Brenner and Edward Garboczi for useful conversations, Holly Rushmier for assistance in imaging results from simulations, and especially Joseph B. Hubbard for carefully reading the text and making useful comments.

Symbols

c	local concentration
C	macroscopically averaged concentration
D_m	molecular diffusion constant
D_h	macroscopic diffusion coefficient
D_p	molecular diffusion constant in pore space
D_s	molecular diffusion constant in solid region
D_L	longitudinal dispersion coefficient
D_T	transverse dispersion coefficient
E	electric field
F	Faraday's constant
p	pressure
Pe	Peclet number
v	fluid velocity
v_i	ion velocity
V	volume averaged velocity
z	ion charge number
η	fluid viscosity
ν	ion mobility
ϕ	porosity
σ_b	bulk conductivity
σ_f	conductivity of fluid

References

[1] P. Wong, Phys. Today, 41 (1988) 24.
[2] F.A.L. Dullien, Porous Media: Fluid Transport and Pore Structure, Academic Press, San Diego, CA, 1992.
[3] A.E. Scheidegger, The Physics of Flow Through Porous Media, 2nd edn., University of Toronto Press, 1974.
[4] P.M. Adler, Porous Media: Geometry and Transports, Butterworth-Heinemann, Boston, MA, 1992.
[5] H.E. Stanley and N. Ostrowsky (Editors), Random Fluctuations and Pattern Growth: Experiments Models, Kluwer Academic Publishers, Netherlands, 1988.

[6] T. Vicsek, Fractal Growth Phenomena, World Scientific, Singapore, 1989.
[7] F. Family and T. Vicsek (Editors), Dynamics of Fractal Surfaces, World Scientific, Singapore, 1991.
[8] J.P. Stokes, D.A. Weitz, J.P. Gollub, A. Dougherty, M.O. Robbins, P.M. Chaikin and H.M. Lindsay, Phys. Rev. Lett., 57 (1986) 1718.
[9] See, e.g., J. Feder, Fractals, Plenum, New York, 1988.
[10] G.D. Doolen, Lattice Gas Methods: Theory, Applications, and Hardware, Elsevier Science Publishers, Amsterdam, 1991.
[11] V.K. Horvath, F. Family and T. Vicsek, Phys. Rev. Lett., 65 (1990) 1388.
[12] K.J. Måløy, J. Feder, F. Boger and T. Jøssang, Phys. Rev. Lett., 61 (1988) 2925.
[13] M.A. Rubio, C. Edwards, A. Dougherty and J.P. Gollub, Phys. Rev. Lett., 63 (1989) 1685.
[14] Many recent results and important references concerning hydrodynamic dispersion in porous media are given in articles included in a special issue titled "Fractal Dispersion and Diffusion", Transport in Porous Media, Vol. 13, No. 1, Oct. 1993. Also see M. Sahimi, Rev. Mod. Phys., 65 (1993) 1393.
[15] In this preliminary study the partitioning of the solute is achieved by requiring continuity of the molecular diffusive flux at the solid–pore interface. Perhaps a more scrupulous aproach would introduce the notion of "partition coefficients", the numerical values of which are determined by thermodynamic or quasi-thermodynamic arguments. See, for instance, H. Brenner and D.A. Edwards, Macroscopic Transport, Butterworth Heinemann, Stoneham, MA, 1993.
[16] M. Sahimi and A.O. Imdakm, J. Phys. A: Math. Gen., 21 (1988) 3833.
[17] J. Salles, J.-F. Thovert, R. Delannay, L. Prevors, J.-L. Auriault and P.M. Adler, Phys. Fluids A, 5 (10) (1993) 2348.
[18] S. Redner, J. Koplik and D. Wilkinson, J. Phys: Math. Gen., 20 (1987) 1543.
[19] N. Martys and E.J. Garboczi, Phys. Rev. B, 46 (1992) 6080.
[20] E.M. Purcell, Electricity and Magnetism, McGraw-Hill, New York, 1965.
[21] R. Peyret and T.D. Taylor, Computational Methods for Fluid Flow, Springer-Verlag, New York, 1983.
[22] J.F. Hawley, L. Smarr and J.R. Wilson, Astrophys. J. Suppl. Ser., 55 (1984) 211.
[23] J. Centralla and J.R. Wilson, Astrophys. J. Suppl. Ser., 54 (1984) 229.
[24] R.K.-C. Chan and R.L. Street, J. Comput. Phys., 6 (1970) 68.
[25] W.H. Press, B.P. Flannery, S.A. Teukolsky and W.T. Vetterling, Numerical Recipes, Cambridge University Press, New York, 1989, p. 54.
[26] M. Muscat, The Flow of Homogeneous Fluids Through Porous Media, McGraw-Hill, New York, 1937.
[27] The physical assumption of insulating, uncharged discs automatically eliminates the possibility of an electrical double layer. We therefore ignore electrokinetic phenomena associated with hydrodynamic effects which are inducted by the interaction of the external field with mobile charges in an "electric double layer" surrounding the discs. For further reference see, R.J. Hunter, Zeta Potential in Colloid Science: Principles and Applications, Academic Press, London, 1981.
[28] R.F. Probstein and R.E. Hicks, Science, 260 (1993) 498.
[29] R. Lenormand, private communication. E. Charlaix, J.-P. Hulin, C. Leroy and C. Zarcone, J. Phys. D: Appl. Phys., 21 (1988) 1727.
[30] D.L. Koch and J. Brady, Phys. Fluids A, 1 (1989) 47; S. Redner, J. Koplik and D. Wilkison, J. Phys. A: Math. Gen., 20 (1987) 1543; M. Sahimi and A.O. Imdakm, J. Phys. A: Math. Gen., 21 (1988) 3833.